Supplemental Information:

Title: A modeling method for increased precision and scope of directly measurable fluxes at a genome-scale

Authors:

Douglas McCloskey[1], Jamey D. Young[3,4], Sibei Xu[1], Bernhard O. Palsson[1,2], and Adam M. Feist[1,2]

1 Department of Bioengineering, University of California, San Diego, CA 92093, USA.
2 Novo Nordisk Foundation Center for Biosustainability, Technical University of Denmark, 2800 Lyngby, Denmark.
3 Department of Chemical and Biomolecular Engineering, and 4 Department of Molecular Physiology and Biophysics, Vanderbilt University, Nashville, TN 37235-1604, USA
* Corresponding author. AM Feist, Department of Bioengineering, University of California, San Diego, 9500 Gilman Drive, La Jolla, CA 92093-0412, USA.
Tel.: 1 858 534 9592; Fax: 1 858 822 3120; E-mail: afeist@ucsd.edu

Table of Contents:

Figure S-1: Carbon mapping naming convention. A toy example is shown for pyruvate. The compounds included in the example include acetate (ac), carbon dioxide (co2), and pyruvate (pyr). For each sub-compound that composes another compound, a "_compound number" is appended to the compound name. For example, pyruvate can be composed of carbon dioxide and acetate. Pyruvate can be designated as "co2_0 + ac_0" to specify that pyruvate is composed of 1 carbon dioxide molecule and 1 acetate molecule. Pyruvate can be further broken down to its carbon numbers. This can be described by adding a "_element position" to each sub-compound. Brackets are used to group all carbons that come from a single compound for easier reading.

"compound"_"compound number"_"element position"

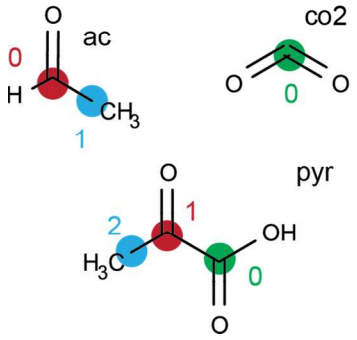

pyr_0 = co2_0 + ac_0
pyr_0 = co2_0_C0 + [ac_0_C0 + ac_0_C1]
pyr_0 = pyr_0_C0 + pyr_0_C1 + pyr_0_C2

ac_0 = pyr_0 - co2_0
ac_0 = co2_0_C0 + [ac_0_0 + ac_0_C1] - co2_0_C0
ac_0 = [ac_0_C0 + ac_0_C1]

Figure S-2: Carbon mapping naming convention. An example of constructing a complex macromolecule from precursor and intermediate metabolites.

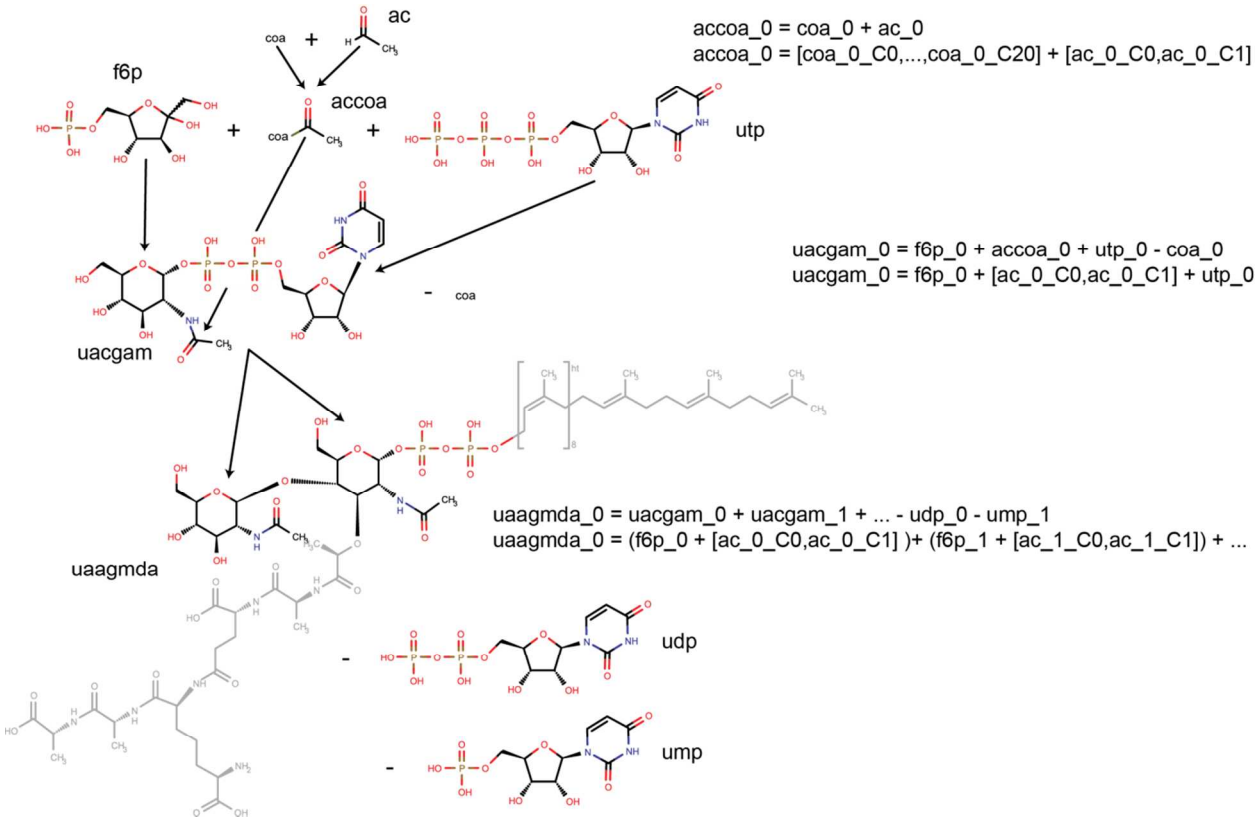

Figure S-3: Differences in estimated net flux values found between different MFA models. Fold-changes over observable net flux values calculated using the same data set and different models compared to iDM2014 that were significant as determined by 95% confidence intervals are shown.

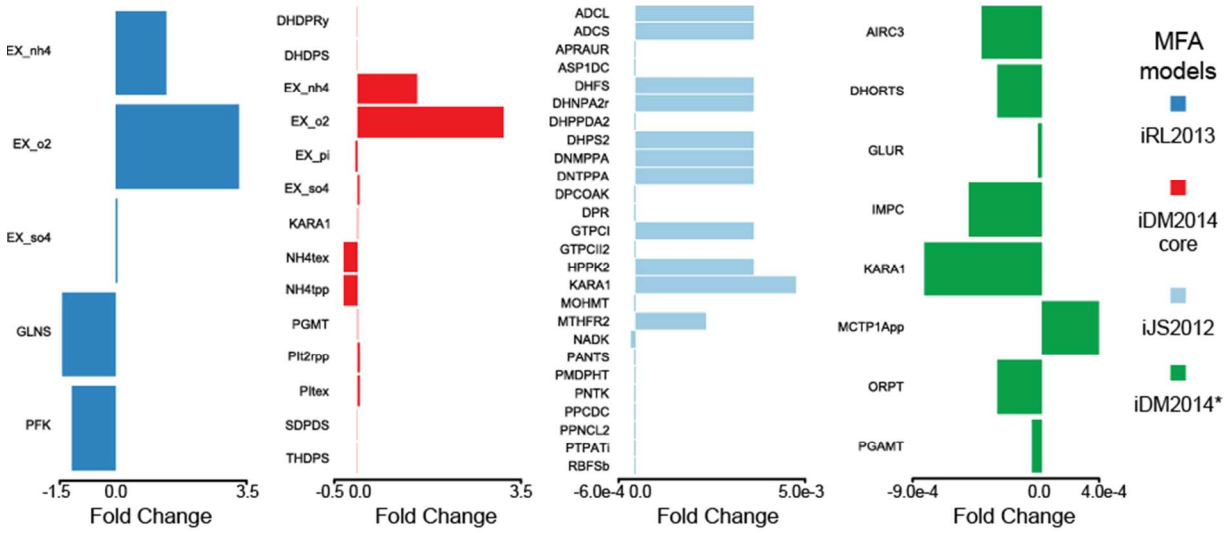

Figure S-4: Model robustness to incorrect atom mappings and addition or removal of non-essential reactions. The fold-change over net flux values calculated using iDM2014 are shown. iDM2014_glyc,26dap denotes iDM2014 with incorrect symmetry for glycerol, L,L-diaminopimelate , and meso-diaminopimelate. iDM2014_26dap denotes iDM2014 with incorrect symmetry for L,L-diaminopimelate , and meso-diaminopimelate. iDM2014_hex denotes iDM2014 with addition of the ability to transport glucose into the cell via the action of hexokinase, and iDM2014_pfl denotes iDM2014 without pyruvate formate lyase.

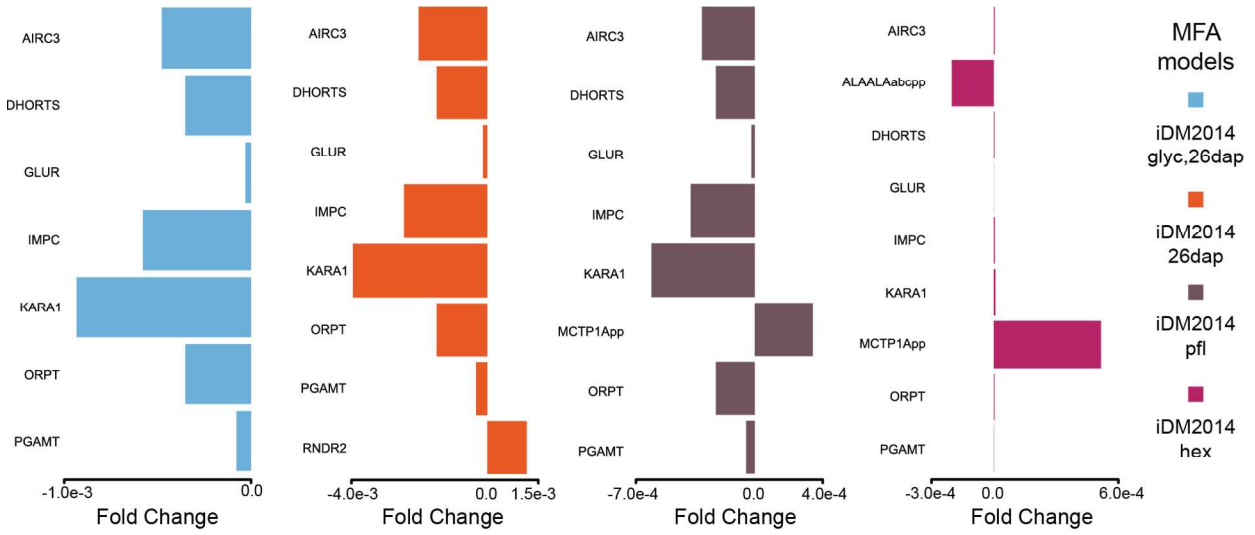

Figure S-5: Net flux values calculated with and without non-essential reactions. Flux predictions, including precision, of key reactions in central carbohydrate metabolism calculated using the same data set and different models. Circles represent the best net flux estimate; whiskers represent +/- the standard deviation as calculated from 95% confidence intervals. All flux values are normalized to net glucose uptake. iDM2014_hex denotes iDM2014 with addition of the ability to transport glucose into the cell via the action of hexokinase, and iDM2014_pfl denotes iDM2014 without pyruvate formate lyase.

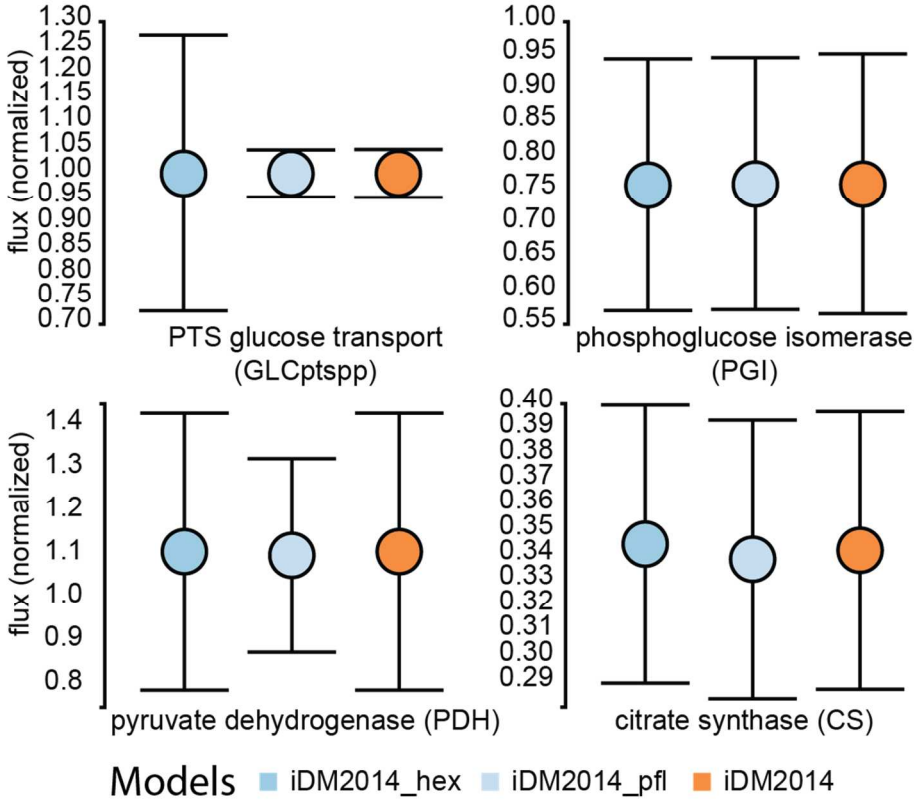

Table S-1: Fitted net fluxes for all flux simulations

Table S-2: Fitted net fluxes for model robustness simulations

Table S-3: Measured fluxes.

Table S-4: Measured MS MIDs.

Table S-5: Reaction list and carbon mapping for all models. Note that Ec_biomass_iJO1366_WT_53p95M for the iDM2014 model is split across two lines due to its length.

Table S-6: Symmetric metabolite mappings for all models.

Table S-7: Effect of incorrect carbon mapping symmetry on flux estimation precision.

Table S-8: Metabolic engineering targets of high value and peripheral pathways that can be directly measured using genome-scale MFA.

Products	Pathways	Reference
Heterologous DNA	Purine biosynthesis	[1]
Heterologous DNA	Pyrimidine biosynthesis	[1]
Caratenoids	Isoprenoid biosynthesis (DXP pathway)	[2,3]
Artemisinin	Isoprenoid biosynthesis (DXP pathway)	[4-7]
Taxol	Isoprenoid biosynthesis (DXP pathway)	[8,9]
Free fatty acids	Lipid biosynthesis	[10-12]
Free fatty acids	Coenzyme A biosynthesis	[10-12]
Riboflavin	FAD biosynthesis	[13]
Folic acid	Folate biosynthesis	[14]
C5 alcohols	Isoprenoid biosynthesis (DXP pathway)	[15]
Putrescine	Putrescine biosynthesis	[16]
Cadaverine	Putrescine biosynthesis	[17]
CoQ10	ubiquinone biosynthesis	[18]
CoQ10	Isoprenoid biosynthesis (DXP pathway)	[18]
CoQ10	aromatic amino acid biosynthesis	[18]
CoQ8	ubiquinone biosynthesis	[19]
CoQ8	Isoprenoid biosynthesis (DXP pathway)	[19]
CoQ8	aromatic amino acid biosynthesis	[19]
Vitamin K	menaquinone biosythesis	[20]
Vitamin K	Isoprenoid biosynthesis (DXP pathway)	[20]
Vitamin K	aromatic amino acid biosynthesis	[20]
phenol	aromatic amino acid biosynthesis	[21]
Shikimate and chorismate	aromatic amino acid biosynthesis	[22-24]
L-tyrosine, L-phenylalanine, and L-tryptophan	aromatic amino acid biosynthesis	[25-28]
L-threonine	aromatic amino acid biosynthesis	[29]
Lycopene	Isoprenoid biosynthesis (DXP pathway)	[30,31]
Cinnamic and p-hydroxycinnamic acid	aromatic amino acid biosynthesis	[32]
L-DOPA	aromatic amino acid biosynthesis	[33]
Melanin	aromatic amino acid biosynthesis	[34]

Table S-9: A comparison of precision between models and estimated flux values for representative core fluxes reported in this study compared to estimated flux values reported in Gopalakrishnan et al, 2015[35] using two different tracer schemes.

Table S-10: List of metabolites and MIDs included in the fit of the genome-scale model.

fragment_id	met_id	fragment_formula	scan_type
13dpg_c_C3H7O10P2_MRM	13dpg_c	C3H7O10P2	MRM
3pg_c_C2H6O5P_EPI	3pg_c	C2H6O5P	EPI
3pg_c_C3H6O7P_EPI	3pg_c	C3H6O7P	EPI
3pg_c_C3H6O7P_MRM	3pg_c	C3H6O7P	MRM
6pgc_c_C6H10O9P_EPI	6pgc_c	C6H10O9P	EPI
6pgc_c_C6H12O10P_EPI	6pgc_c	C6H12O10P	EPI
6pgc_c_C6H12O10P_MRM	6pgc_c	C6H12O10P	MRM
accoa_c_C10H12N5O9P2_EPI	accoa_c	C10H12N5O9P2	EPI
accoa_c_C10H14N5O10P2_EPI	accoa_c	C10H14N5O10P2	EPI
accoa_c_C13H23N2O10P2S_EPI	accoa_c	C13H23N2O10P2S	EPI
accoa_c_C23H37N7O17P3S_MRM	accoa_c	C23H37N7O17P3S	MRM
acon_DASH_C_c_C4H5O2_EPI	acon_DASH_C_c	C4H5O2	EPI
acon_DASH_C_c_C5H5O4_EPI	acon_DASH_C_c	C5H5O4	EPI
acon_DASH_C_c_C5H5O4_MRM	acon_DASH_C_c	C5H5O4	MRM
acon_DASH_C_c_C6H3O5_EPI	acon_DASH_C_c	C6H3O5	EPI
acon_DASH_C_c_C6H5O6_EPI	acon_DASH_C_c	C6H5O6	EPI
acon_DASH_C_c_C6H5O6_MRM	acon_DASH_C_c	C6H5O6	MRM
akg_c_C2HO3_EPI	akg_c	C2HO3	EPI
akg_c_C4H5O3_EPI	akg_c	C4H5O3	EPI
akg_c_C4H5O3_MRM	akg_c	C4H5O3	MRM
akg_c_C5H5O5_MRM	akg_c	C5H5O5	MRM
amp_c_C10H13N5O7P_EPI	amp_c	C10H13N5O7P	EPI
amp_c_C10H13N5O7P_MRM	amp_c	C10H13N5O7P	MRM
amp_c_C5H4N5_EPI	amp_c	C5H4N5	EPI
amp_c_C5H8O7P_EPI	amp_c	C5H8O7P	EPI
asp_DASH_L_c_C3H6NO2_EPI	asp_DASH_L_c	C3H6NO2	EPI
asp_DASH_L_c_C3H6NO2_MRM	asp_DASH_L_c	C3H6NO2	MRM
asp_DASH_L_c_C4H3O4_EPI	asp_DASH_L_c	C4H3O4	EPI
asp_DASH_L_c_C4H6NO4_EPI	asp_DASH_L_c	C4H6NO4	EPI
asp_DASH_L_c_C4H6NO4_MRM	asp_DASH_L_c	C4H6NO4	MRM
atp_c_C10H15N5O13P3_MRM	atp_c	C10H15N5O13P3	MRM
atp_c_C5H4N5_EPI	atp_c	C5H4N5	EPI
dhap_c_C3H6O6P_EPI	dhap_c	C3H6O6P	EPI
dhap_c_C3H6O6P_MRM	dhap_c	C3H6O6P	MRM
fad_c_C27H32N9O15P2_MRM	fad_c	C27H32N9O15P2	MRM
fdp_c_C6H10O8P_EPI	fdp_c	C6H10O8P	EPI
fdp_c_C6H13O12P2_EPI	fdp_c	C6H13O12P2	EPI
fdp_c_C6H13O12P2_MRM	fdp_c	C6H13O12P2	MRM
fdp_c_C6H8O7P_EPI	fdp_c	C6H8O7P	EPI
g1p_c_C6H12O9P_MRM	g1p_c	C6H12O9P	MRM

g6p_c_C2H4O5P_EPI	g6p_c	C2H4O5P	EPI
g6p_c_C4H8O7P_EPI	g6p_c	C4H8O7P	EPI
g6p_c_C6H12O9P_EPI	g6p_c	C6H12O9P	EPI
g6p_c_C6H12O9P_MRM	g6p_c	C6H12O9P	MRM
glu_DASH_L_c_C4H8NO2_EPI	glu_DASH_L_c	C4H8NO2	EPI
glu_DASH_L_c_C5H6NO3_EPI	glu_DASH_L_c	C5H6NO3	EPI
glu_DASH_L_c_C5H6NO3_MRM	glu_DASH_L_c	C5H6NO3	MRM
glu_DASH_L_c_C5H8NO4_EPI	glu_DASH_L_c	C5H8NO4	EPI
glu_DASH_L_c_C5H8NO4_MRM	glu_DASH_L_c	C5H8NO4	MRM
glyc3p_c_C3H8O6P_EPI	glyc3p_c	C3H8O6P	EPI
glyc3p_c_C3H8O6P_MRM	glyc3p_c	C3H8O6P	MRM
glyclt_c_C2H3O3_EPI	glyclt_c	C2H3O3	EPI
glyclt_c_C2H3O3_MRM	glyclt_c	C2H3O3	MRM
icit_c_C5H3O3_EPI	icit_c	C5H3O3	EPI
icit_c_C5H3O3_MRM	icit_c	C5H3O3	MRM
icit_c_C6H5O6_EPI	icit_c	C6H5O6	EPI
icit_c_C6H7O7_EPI	icit_c	C6H7O7	EPI
icit_c_C6H7O7_MRM	icit_c	C6H7O7	MRM
mal_DASH_L_c_C4H3O4_EPI	mal_DASH_L_c	C4H3O4	EPI
mal_DASH_L_c_C4H3O4_MRM	mal_DASH_L_c	C4H3O4	MRM
mal_DASH_L_c_C4H5O5_EPI	mal_DASH_L_c	C4H5O5	EPI
mal_DASH_L_c_C4H5O5_MRM	mal_DASH_L_c	C4H5O5	MRM
met_DASH_L_c_C5H10NO2S_MRM	met_DASH_L_c	C5H10NO2S	MRM
met_DASH_L_c_CH3S_MRM	met_DASH_L_c	CH3S	MRM
pep_c_C3H4O6P_MRM	pep_c	C3H4O6P	MRM
phe_DASH_L_c_C9H10NO2_MRM	phe_DASH_L_c	C9H10NO2	MRM
phe_DASH_L_c_C9H7O2_MRM	phe_DASH_L_c	C9H7O2	MRM
phpyr_c_C7H7_MRM	phpyr_c	C7H7	MRM
phpyr_c_C9H7O3_MRM	phpyr_c	C9H7O3	MRM
prpp_c_C5H12O14P3_MRM	prpp_c	C5H12O14P3	MRM
pyr_c_C3H3O3_MRM	pyr_c	C3H3O3	MRM
r5p_c_C5H10O8P_MRM	r5p_c	C5H10O8P	MRM
ru5p_DASH_D_c_C5H10O8P_MRM	ru5p_DASH_D_c	C5H10O8P	MRM
s7p_c_C7H14O10P_MRM	s7p_c	C7H14O10P	MRM
skm_c_C6H5O_MRM	skm_c	C6H5O	MRM
succ_c_C3H5O2_EPI	succ_c	C3H5O2	EPI
succ_c_C4H3O3_MRM	succ_c	C4H3O3	MRM
succ_c_C4H5O4_MRM	succ_c	C4H5O4	MRM
thr_DASH_L_c_C2H4NO2_MRM	thr_DASH_L_c	C2H4NO2	MRM
thr_DASH_L_c_C4H8NO3_MRM	thr_DASH_L_c	C4H8NO3	MRM
ump_c_C4H3N2O2_EPI	ump_c	C4H3N2O2	EPI

ump_c_C9H12N2O9P_EPI	ump_c	C9H12N2O9P	EPI
ump_c_C9H12N2O9P_MRM	ump_c	C9H12N2O9P	MRM

Table S-11: A comparison of MFA estimated flux ranges to FVA estimated flux ranges for iDM2014. MFA flux ranges were calculated as the difference between 95% confidence intervals, while the FVA flux ranges were calculated as the difference between the minimum and maximum flux. Differences in fluxes between the two methods were considered statistically significant if the flux ranges between the two methods did not overlap. Note that the lack of statistically significant fluxes between MFA and FVA estimated fluxes for core metabolism is due to the large flux ranges of FVA for core metabolism reactions.

	MFA vs. FVA relative flux range difference	**MFA vs. FVA statistically significant fluxes**
All reactions	6.59%	26.32%
Core metabolism	34.45%	0.00%
Peripheral metabolism	2.56%	27.10%

Supplemental Methods:

Peripheral metabolism reduction:

The first part of the peripheral metabolism reduction procedure involved identifying all reactions of peripheral metabolism that could be lumped into a single reaction without having an effect on growth rate. Reactions that were linear and correlated that could be lumped into a single reaction were identified using pFBA. A single lumped reaction from the pool of lumped reactions was iteratively incorporated into the network to test for a change in growth rate. Lumped reactions that changed the growth rate were excluded from the pool and another lumped reaction tested. Lumped reactions that did not change the growth rate were left in the network and a new pool of lumped reactions was identified using the new network. This process was repeated until no further lumped reactions that did not change the growth rate could be identified.

The second part of the peripheral metabolism reduction procedure involved pruning no flux reactions and removing equivalent alternate pathways. No flux and equivalent pathways were removed using a combination of FVA and pFBA. One potential problem when using pFBA is the preferential selection of the shortest pathway. This can alter cofactor balances, which could have an effect on simulation results. Consequently, cases where equivalent alternate pathways existed with different cofactor usages were manually reviewed before removing from the network. Notable examples include fatty acid metabolism and deoxyribonucleotide biosynthesis. For the former case, pFBA selects the reverse-beta oxidation pathway for fatty acid biosynthesis to conserve NADPH. This is physiologically not correct[36]. For the latter, specific ribonucleotide ruductases exist that are expressed as a function of the amount of oxygen present as well as under certain stress conditions[36-38]. pFBA does not always select the appropriate ribonucleotide reductase. For this reason, the physiologically correct fatty acid biosynthetic pathway as well as the physiologically correct deoxyribonucleotide biosynthetic pathways was manually enforced.

Modifications to iRL2013:

Reactions and metabolite identifiers in iRL2013 [39] were substituted for corresponding or similar identifiers found in iJO1366. iRL2013 does not explicitly include many of the metabolites measured in this study. For this reason, measurements corresponding to phenylpyruvate, glycolate, PRPP, glycerol 3-phosphate, aconitate-C and 1,3 disphosphoglycerate were labeled as L-phenylalanine, glyoxylate, ribose 5-phosphate, dihydroxyacetone phosphate, citrate, and 3pg , respectively, during the flux estimation procedure.

Modifications to iJS2012:

In the published iJS2012 model [40], the carbon mappings for glycerol (metabolite ids glyc_c and glyc_e), L,L-diaminopimelate (metabolite id 26dap_DASH_LL_c), and meso-diaminopimelate (metabolite id 26dap_DASH_M_c) are treated as symmetric. These designations of symmetry are not correct. Glycerol is pro-chiral [37] and L,L-diaminopimelate and meso-diaminopimelate exhibit stereo-symmetry. The carbon mappings for glycerol, L,L-diaminopimelate, and meso-diaminopimelate are treated as non-symmetric in the models presented in this work.

Reconciliation of reaction names between models:

For purposes of comparing the models, names in the iRL2013 model were replaces with corresponding BiGG reaction identifiers to a reasonable extent. Several lumped reactions (e.g., HisSYN) were not reconciled due to stoichiometric differences in the reactions between the models, and were left as is.

Metabolic Flux Analysis:

The degrees of freedom (DOF) were calculated as follows: $DOF = Measured\ MIDs + Measured\ Fluxes - Free\ fluxes$. Confidence intervals were calculated using a method similar to that described in Antoniewicz 2006[41] as encoded in INCA [42]. Standard deviations were calculated based off of 95% confidence intervals as described in Antoniewicz 2006[41] as follows: $Standard\ Deviation = (upper\ bound - lower\ bound)/4$. Observable fluxes were determined as described in Choi 2011[43]. Observable fluxes were those where the estimated flux value was at least four times larger than the 95% confidence interval and did not include the value zero. Standard deviations of observable fluxes were used to compare the precision of each model. Observable fluxes instead of all fluxes were used in order to prevent artificially degrading the precision of the smaller models. Significant difference between fluxes was determined by the 95% confidence intervals.

Standard deviations from biological triplicates were used to weight the errors of the measured uptake, secretion, and growth rates. The uptake, secretion, and growth rates were measured for wild-type *E. coli* on unlabeled glucose M9 minimal media as described previously[44]. Standard deviations of biological triplicates measured in analytical duplicate (n=6) or the accuracy as determined from unlabeled glucose labeling experiments [45] were used to weight the errors of the isotope distributions. In addition, the error-weighted residuals of the fit had to be from a normal distribution (as determined by a Lilliefors test) before flux estimations were considered for analysis. The minimum weight for any isotope measurements was set at 0.001. Flux estimates for iRL2013, iDM2014_core, and iJS2012 were calculated from the best estimate of 10, 100, and 100 re-initializations, respectively. The best estimated flux served as the starting point for the parameter estimation procedure that calculated the 95% confidence intervals. 500 re-initializations were used for iDM2014 in order to minimize the chance of finding a local instead of global optimal estimate due to the larger size of the network.

Representative fluxes:

A set of representative net fluxes that were common to all models were used for comparison. The representative reactions are the following: ATPM, PGI, MDH, EDA, EDD, SUCOAS, PGL, PGM, PGK, ACONTa, ACONTb, GLCptspp, FUM, ENO, SUCDi, RPE, AKGDH, PDH, GAPD, MALS, CS, GND, PPC, TPI, RPI, PYK, ME1, ME2, TALA, ICDHyr, FBA, PFK, ICL, and PPCK.

Supplemental Discussion:

Model sensitivity and robustness

As noted previously, biochemical references for atom mappings from databases and previously published models are often incomplete and may contain in-accuracies. For example, the carbon mappings for glycerol are designated as symmetric in the iJS2012 model [40] as well as in a number of reactions in the EcoCyc database [46]. The carbon mappings for reactions involving L,L-diaminopimelate (metabolite id 26dap_DASH_LL_c), and meso-diaminopimelate (metabolite id 26dap_DASH_M_c) are also incorrectly treated as symmetric in the iJS2012 model. Given the ease at which one can propogate errors from published and well-known resources, the effect of incorporating incorrect mapping symmetry on flux estimation accuracy and precision was explored. The iDM2014 model was simulated with the carbon mappings for glycerol, L,L-diaminopimelat, and meso-diaminopimelate treated as symmetric or L,L-diaminopimelat and meso-diaminopimelate as symmetric and compared to the iDM2014 model with glycerol, L,L-diaminopimelat, and meso-diaminopimelate treated as non-symmetric (Table S-7). Only minor differences in estimated flux values were found compared to iDM2014, which included seven and eight observable net reactions, respectively, with a fold-change less than 1e-3 (Supplemental Figure S-4). The number of observable fluxes was found to increase and the precision was found to improve either for all net fluxes or a subset of core net fluxes as fewer incorrect symmetric carbon mappings were included in the network.

The robustness of the model to adding or removing non-essential reactions that result in equivalent carbon mappings for the product metabolites was tested (Supplemental Figure S-4). The effect of adding the ability to transport glucose passively over the periplasmic membrane and convert to glucose-6-phosphate via the action of hexokinase (iDM2014_hex) or removing the alternate conversion of pyruvate to Acetyl-CoA via the action of pyruvate formate lyase (iDM2014_pfl) was tested. Only minor flux difference were found compared to iDM2014, which included seven and seven observable net reactions, respectively, with a fold-change less than 1e-3 (Supplemental Figure S-4). In the former case, the flux values for glucose import via the glucose phosphotransferase system did not change, but a loss of precision was found (Supplemental Figure S-5). The precision of downstream reactions phosphoglucose isomerase and 6-phosphogluconolactonase were not affected. In the latter case, the flux values for the pyruvate dehydrogenase complex were not affected, but an increase in precision was found. The precision of the downstream reaction citrate synthase was not affected (Supplemental Figure S-5). These changes indicate that when using the genome-scale model, precision can be improved by removing non-essential reactions without affecting the accuracy of the flux predictions.

These examples show that the overall accuracy of the model can be maintained even if errors in metabolite mappings are included or non-essential reactions are added or omitted at the price of reduced precision.

Statistically significant and observable flux differences between the MFA models:

Minor net flux differences for observable reactions between models were found (Supplemental Figure 3). Most of these differences were not statistically significant. Of those that were, most were found to be due to discrepancies in definitions of the forward versus the reverse reaction (e.g., EX_o2 which corresponds to the transport of O2) or resulted in a fold change less than 0.005. Two interesting examples that were found to be attributed to model differences are described below.

Net flux values estimated by iRL013 for phospho-fructose kinase (PFK) were found to be significantly different to those estimated by iDM2014_core and iDM2014. This was due to the fact that fructose 1,6-bisphosphatase (FBP) is not included in the published iRL2013 model. By excluding this reaction, the recycling of fructose 1,6-bisphosphate to fructose 6-phosphate is not allowed. Net flux values estimated by iRL2013 for glutamine synthetase (GLNS) were found to be significantly different to

those estimated by iDM2014_core and iDM2014. This could be due to the fact that the published iRL2013 utilizes glutamate dehydrogenase to synthesize glutamate instead of the actions of glutamine synthetase and glutamate synthase to synthesize glutamate. There is evidence to show that due to the higher Km of glutamate dehydrogenase and alternate regulation of glutamate dehydrogenase and glutamate synthase, glutamate dehydrogenase is more actively expressed when nitrogen is abundant in the media and glutamate synthesase is more active when nitrogen is limited in the media[47]. The cultures were not grown in ammonia excess in this study. This leads one to hypothesize that the flux values estimated by iDM014 for GLNS are the physiologically correct values.

Increased scope of measured flux values:

Another major benefit to using a genome-scale model for MFA is the direct calculation of flux balance around Acetyl-CoA, ATP, and NADPH. This is important as Acetyl-CoA and ATP are the major energy sources and NADPH is the major reducing source for native and non-native pathways such as in the production of free-fatty acids for biofuels [10-12]. The success or failure of several metabolic engineering designs has relied upon redirecting flux to maintain an optimal balance of the charged and uncharged state of these cofactors [48-50]. Thus, a genome-scale model for MFA would help guide engineering strategies aimed at manipulating the flux to and from these cofactors.

Supplemental Files:

File 1: A high resolution flux map of central carbohydrate metabolism for iDM2014. The best net flux value is shown.

File 2: A high resolution flux map of peripheral pathways targeted by metabolic engineering for iDM2014. The best net flux value is shown.

References:

(1) Fuentes, L.; Lara, A.; Martinez, L.; Ramirez, O.; Martinez, A.; Bolivar, F.; Gosset, G. *Microbial Cell Factories* **2013**, *12*, 42.
(2) Matthews, P. D.; Wurtzel, E. T. *Appl Microbiol Biotechnol* **2000**, *53*, 396-400.
(3) Yuan, L. Z.; Rouvière, P. E.; LaRossa, R. A.; Suh, W. *Metabolic Engineering* **2006**, *8*, 79-90.
(4) Anthony, J. R.; Anthony, L. C.; Nowroozi, F.; Kwon, G.; Newman, J. D.; Keasling, J. D. *Metab Eng* **2009**, *11*, 13-19.
(5) Martin, V. J.; Pitera, D. J.; Withers, S. T.; Newman, J. D.; Keasling, J. D. *Nat Biotechnol* **2003**, *21*, 796-802.
(6) Newman, J. D.; Marshall, J.; Chang, M.; Nowroozi, F.; Paradise, E.; Pitera, D.; Newman, K. L.; Keasling, J. D. *Biotechnol Bioeng* **2006**, *95*, 684-691.
(7) Pitera, D. J.; Paddon, C. J.; Newman, J. D.; Keasling, J. D. *Metab Eng* **2007**, *9*, 193-207.
(8) Ajikumar, P. K.; Xiao, W.-H.; Tyo, K. E. J.; Wang, Y.; Simeon, F.; Leonard, E.; Mucha, O.; Phon, T. H.; Pfeifer, B.; Stephanopoulos, G. *Science* **2010**, *330*, 70-74.
(9) Huang, Q.; Roessner, C. A.; Croteau, R.; Scott, A. I. *Bioorganic & Medicinal Chemistry* **2001**, *9*, 2237-2242.
(10) Lu, X.; Vora, H.; Khosla, C. *Metabolic Engineering* **2008**, *10*, 333-339.
(11) Steen, E. J.; Kang, Y.; Bokinsky, G.; Hu, Z.; Schirmer, A.; McClure, A.; del Cardayre, S. B.; Keasling, J. D. *Nature* **2010**, *463*, 559-562.
(12) Dellomonaco, C.; Clomburg, J. M.; Miller, E. N.; Gonzalez, R. *Nature* **2011**, *476*, 355-359.
(13) Lin, Z.; Xu, Z.; Li, Y.; Wang, Z.; Chen, T.; Zhao, X. *Microb Cell Fact* **2014**, *13*, 104.
(14) Zhu, T.; Koepsel, R.; Domach, M. M.; Ataai, M. M. In *Fermentation Biotechnology*; American Chemical Society, 2003, pp 207-219.
(15) George, K. W.; Thompson, M. G.; Kang, A.; Baidoo, E.; Wang, G.; Chan, L. J. G.; Adams, P. D.; Petzold, C. J.; Keasling, J. D.; Soon Lee, T. *Sci. Rep.* **2015**, *5*.
(16) Qian, Z.-G.; Xia, X.-X.; Lee, S. Y. *Biotechnology and Bioengineering* **2009**, *104*, 651-662.
(17) Qian, Z.-G.; Xia, X.-X.; Lee, S. Y. *Biotechnology and Bioengineering* **2011**, *108*, 93-103.
(18) Cluis, C. P.; Ekins, A.; Narcross, L.; Jiang, H.; Gold, N. D.; Burja, A. M.; Martin, V. J. J. *Metabolic Engineering* **2011**, *13*, 733-744.
(19) Xu, W.; Yang, S.; Zhao, J.; Su, T.; Zhao, L.; Liu, J. *Journal of Industrial Microbiology & Biotechnology* **2014**, *41*, 1297-1303.
(20) Kong, M. K.; Lee, P. C. *Biotechnology and Bioengineering* **2011**, *108*, 1997-2002.
(21) Kim, B.; Park, H.; Na, D.; Lee, S. Y. *Biotechnology Journal* **2014**, *9*, 621-629.
(22) Cortes-Tolalpa, L.; Gutierrez-Rios, R.; Martinez, L.; de Anda, R.; Gosset, G.; Bolivar, F.; Escalante, A. *Microbial Cell Factories* **2014**, *13*, 28.
(23) Chen, X.; Li, M.; Zhou, L.; Shen, W.; Algasan, G.; Fan, Y.; Wang, Z. *Bioresource Technology* **2014**, *166*, 64-71.
(24) Floras, N.; Xiao, J.; Berry, A.; Bolivar, F.; Valle, F. *Nat Biotech* **1996**, *14*, 620-623.
(25) Juminaga, D.; Baidoo, E. E. K.; Redding-Johanson, A. M.; Batth, T. S.; Burd, H.; Mukhopadhyay, A.; Petzold, C. J.; Keasling, J. D. *Applied and Environmental Microbiology* **2012**, *78*, 89-98.
(26) Na, D.; Yoo, S. M.; Chung, H.; Park, H.; Park, J. H.; Lee, S. Y. *Nat Biotech* **2013**, *31*, 170-174.
(27) Ikeda, M. *Appl Microbiol Biotechnol* **2006**, *69*, 615-626.
(28) Yakandawala, N.; Romeo, T.; Friesen, A. D.; Madhyastha, S. *Appl Microbiol Biotechnol* **2008**, *78*, 283-291.
(29) Lee, K. H.; Park, J. H.; Kim, T. Y.; Kim, H. U.; Lee, S. Y. *Mol Syst Biol* **2007**, *3*, 149.
(30) Alper, H.; Jin, Y.-S.; Moxley, J. F.; Stephanopoulos, G. *Metabolic Engineering* **2005**, *7*, 155-164.
(31) Alper, H.; Miyaoku, K.; Stephanopoulos, G. *Nat Biotech* **2005**, *23*, 612-616.
(32) Vargas-Tah, A.; Martinez, L.; Hernandez-Chavez, G.; Rocha, M.; Martinez, A.; Bolivar, F.; Gosset, G. *Microbial Cell Factories* **2015**, *14*, 6.
(33) Muñoz, A.; Hernández-Chávez, G.; de Anda, R.; Martínez, A.; Bolívar, F.; Gosset, G. *Journal of Industrial Microbiology & Biotechnology* **2011**, *38*, 1845-1852.
(34) Chavez-Bejar, M.; Balderas-Hernandez, V.; Gutierrez-Alejandre, A.; Martinez, A.; Bolivar, F.; Gosset, G. *Microbial Cell Factories* **2013**, *12*, 108.
(35) Gopalakrishnan, S.; Maranas, C. D. *Metabolic Engineering* **2015**, *32*, 12-22.
(36) McCloskey, D.; Gangoiti, J. A.; King, Z. A.; Naviaux, R. K.; Barshop, B. A.; Palsson, B. O.; Feist, A. M. *Biotechnol Bioeng* **2014**, *111*, 803-815.
(37) Nelson, D.; Cox, M. *Lehninger Principles of Biochemistry, Fourth Edition*; W. H. Freeman, 2004.
(38) Boston, T.; Atlung, T. *Journal of Bacteriology* **2003**, *185*, 5310-5313.
(39) Leighty, R. W.; Antoniewicz, M. R. *Metab Eng* **2013**, *20*, 49-55.
(40) Schellenberger, J.; Zielinski, D. C.; Choi, W.; Madireddi, S.; Portnoy, V.; Scott, D. A.; Reed, J. L.; Osterman, A. L.; Palsson, B. *BMC Syst Biol* **2012**, *6*, 9.
(41) Antoniewicz, M. R.; Kelleher, J. K.; Stephanopoulos, G. *Metab Eng* **2006**, *8*, 324-337.
(42) Young, J. D. *Bioinformatics* **2014**, *30*, 1333-1335.

(43) Choi, J.; Antoniewicz, M. R. *Metab Eng* **2011**, *13*, 225-233.
(44) LaCroix, R. A.; Sandberg, T. E.; O'Brien, E. J.; Utrilla, J.; Ebrahim, A.; Guzman, G. I.; Szubin, R.; Palsson, B. O.; Feist, A. M. *Appl Environ Microbiol* **2015**, *81*, 17-30.
(45) Young, J. D.; Allen, D. K.; Morgan, J. A. *Methods Mol Biol* **2014**, *1083*, 85-108.
(46) Latendresse, M.; Malerich, J. P.; Travers, M.; Karp, P. D. *Journal of Chemical Information and Modeling* **2012**, *52*, 2970-2982.
(47) Helling, R. B. *Journal of Bacteriology* **1994**, *176*, 4664-4668.
(48) Chemler, J. A.; Fowler, Z. L.; McHugh, K. P.; Koffas, M. A. *Metab Eng* **2010**, *12*, 96-104.
(49) Fowler, Z. L.; Gikandi, W. W.; Koffas, M. A. *Appl Environ Microbiol* **2009**, *75*, 5831-5839.
(50) Yim, H.; Haselbeck, R.; Niu, W.; Pujol-Baxley, C.; Burgard, A.; Boldt, J.; Khandurina, J.; Trawick, J. D.; Osterhout, R. E.; Stephen, R.; Estadilla, J.; Teisan, S.; Schreyer, H. B.; Andrae, S.; Yang, T. H.; Lee, S. Y.; Burk, M. J.; Van Dien, S. *Nat Chem Biol* **2011**, *7*, 445-452.